

Erythrocytes analysis with a Digital Holographic Microscope

B. Rappaz^a, A. Barbul^b, F. Charrière^c, J. Kühn^c, P. Marquet^d, R. Korenstein^b, C. Depeursinge^c and P. Magistretti^{a,d}

^aEPFL, Brain Mind Institute, Lausanne, 1015, Switzerland

^bDepartment of Physiology and Pharmacology, Sackler Faculty of Medicine, Ramat Aviv 69 978, Tel-Aviv, Israel

^cEcole Polytechnique Fédérale de Lausanne (EPFL), Imaging and Applied Optics Institute, Lausanne, 1015, Switzerland

^dCentre de Neurosciences Psychiatriques, Département de psychiatrie DP-CHUV, Site de Cery, Prilly-Lausanne, 1008, Switzerland
email: Benjamin.Rappaz@epfl.ch

ABSTRACT

Digital holographic microscopy (DHM) is a technique that allows obtaining, from a single recorded hologram, quantitative phase image of living cell with interferometric accuracy (Marquet et al., 2005). Specifically the optical phase shift induced by the specimen on the transmitted wave front can be regarded as a powerful endogenous contrast agent, depending on both the thickness and the refractive index of the sample. We have recently proposed (Rappaz et al., 2005) a new and efficient decoupling procedure allowing to directly obtain separate measurements of the thickness and the integral refractive index of a given living cell. Consequently, it has been possible, for the first time to our knowledge, to accurately measure (with a precision of 0.0003) the mean refractive index of living erythrocytes. On the other hand, the cellular thickness measurements allow to calculate the volume and shape of erythrocytes. In addition, DHM, thanks to its subwavelength phase shift measurements, was found to yield an efficient tool to assess erythrocyte cell membrane fluctuations (ECMF). Typically, ECMF characterized by an amplitude within the range of 45 nm were observed.

Keywords: digital holography, erythrocyte, cell imaging, refractive index

INTRODUCTION

Digital holographic microscopy (DHM) we have developed is a technique allowing to obtain, from a single recorded hologram, quantitative phase images of living cell dynamics with interferometric accuracy (Cuhe et al., 1999). The optical phase shift induced by a given sample on the transmitted wavefront can be regarded as a powerful endogenous contrast agent, as it contains information about both the thickness and the refractive index of the sample. We have proposed (Rappaz et al., 2005) a decoupling procedure, based on a concept initially proposed by (Barer, 1957; Evans and Fung, 1972), allowing to directly calculate from the quantitative phase signal the corresponding cell morphology and integral refractive index related to the intracellular content, notably proteins. This procedure is particularly useful for measuring, in the same experimental conditions, both cell morphology changes and their associated integral refractive index modifications occurring during biological processes (Rappaz et al., 2005).

Erythrocytes are composed (Mazeron et al., 1997) of hemoglobin (32%, refractive index: $n = 1.615$) water (65%, $n = 1.333$) and membrane components (3%, $n = 1.6$) and do not contain any nucleus. They can be characterized by their volume, shape and refractive index. Those parameters, altered in various pathological processes, can be used as good indicators to (Mohandas and Evans, 1994).

CELL PREPARATION

100-150 μ l of blood was drawn from healthy laboratory personnel by fingerpick, collected and diluted at a ratio of 1:10 (v/v) in cold HEP buffer (15 mM HEPES pH 7.4, NaCl 130 mM, KCl 5.4 mM and 10 mM glucose). Blood cells were sedimented at 200 g, 4 °C for 10 min and buffy coat with upper 20% of erythrocytes were gently removed. Red blood cells were washed twice in HEP buffer (1000 g X 2 min at 4 °C). Finally, erythrocytes were suspended in HEPA buffer (15 mM HEPES pH 7.4, 130 mM NaCl, 5.4 mM KCl, 10 mM glucose, 1 mM CaCl₂, 0.5 mM MgCl₂ and 1 mg/ml bovine serum albumin) at 0.2 % hematocrit. The erythrocyte suspension was introduced into the experimental perfusion chamber consisting of two cover glasses separated by spacers 1.2 mm thick, and incubated for 20 min at 37 °C. This allows the erythrocytes to adhere to the glass coverslip. Unattached cells were removed by gently perfusing the chamber with HEPA solution. The chamber was then mounted on the DHM stage and holograms were acquired and reconstructed on-line using custom-made Koala software package. Neither erythrocyte shape transitions nor volume changes were detected during all over the experiment. Only cells displaying a normal biconcave shape were selected for analysis. All

experiments were conducted at room temperature ($\sim 22^\circ\text{C}$). For the decoupling procedure presented later either 60 mM mannitol or 60 mM Nycodenz (Histodenz, Sigma) was added to the HEPA buffer. In addition water was added to preserve the osmolarity of 298 mOsm (measured with a freezing-point osmometer (Roebbling, Germany)).

DIGITAL HOLOGRAPHIC MICROSCOPE EXPERIMENTAL SETUP

The experimental setup is a modified Mach-Zehnder configuration (Figure 1). Light transmitted by the specimen and collected by a microscope objective (MO) forms the object wave \mathbf{O} , which interferes with a reference wave \mathbf{R} to produce the hologram intensity I_H recorded by the digital camera (Figure 1B). Holograms are recorded in an off-axis geometry i.e. the reference wave reaches the CCD camera with a small incidence angle with respect to the propagation direction of the object wave.

A detailed description of the algorithm used for hologram reconstruction and aberration compensation have been previously described in (Colomb et al., 2006; Cuche et al., 1999).

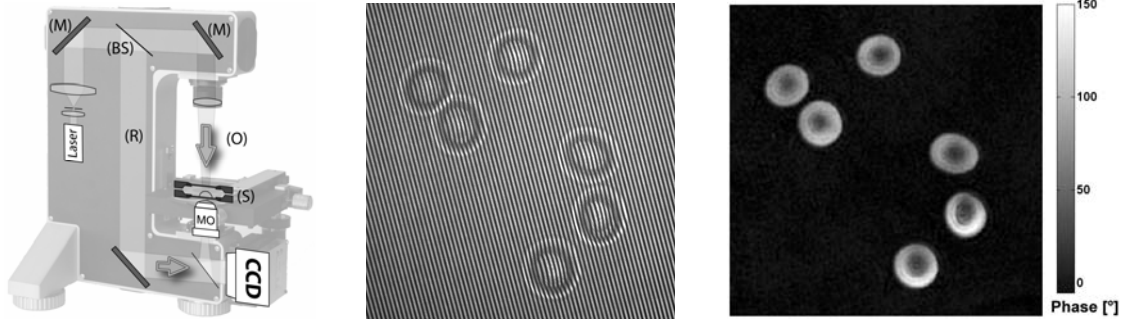


Figure 1 : (A) Basic configuration for digital holographic microscopy (DHM). A VCSEL laser diode produces the coherent light ($\lambda = 663 \text{ nm}$) which is divided by a beam splitter (BS). The specimen (S) is illuminated by one beam through a condenser (C). A microscope objective (MO), 60x, 0.9NA collects the transmitted light and forms the object wave (O) which interferes with a reference beam (R) to produce the hologram recorded by the digital CCD camera (Basler A101f). The sample is mounted in a close perfusion chamber used to apply the different solutions (B) Typical example of a hologram acquired by the camera (512×512 pixels). C. Typical quantitative phase image of erythrocytes.

Briefly, the reconstruction procedure consists in a simulation of the re-illumination of the hologram by a digital reference wave and a numerical correction of the wavefront aberrations induced by the objective and by the off-axis geometry. Hologram processing used in this study performs a numerical reshaping of complex wavefronts and of their propagation, thereby replacing the need for complex opto-mechanical adjustment procedures, and fine alignment of the sample along the optical axis. This allows monitoring living material with a great ease of use.

The acquisition time is currently limited by the exposure time of the camera (down to $\sim 20\mu\text{s}$) and the intensity of the irradiating source. The reconstruction process is achieved in real-time (>15 images/s) using a standard PC computer (Pentium IV, 3.2 GHz). For experiments requiring higher hologram acquisition rates, the reconstruction is achieved off-line at the end of the experiment.

DECOUPLING PROCEDURE

According to Rappaz et al. (2005), the separate measurements of the integral refractive index $\bar{n}_{c,i}$ and the cell thickness have been performed by measuring cell phase mapping, sequentially, in two iso-osmolar perfusion solutions of different refractive indices. Specifically, the refractive index of the second solution is increased by replacing mannitol (a hydrophilic sugar present in the standard perfusion solution) with equal molarity of the hydrophilic molecule Nycodenz. Typically addition of 4% w/v of Nycodenz increases the refractive index of the solution by $\delta n = 0.006$. The different refractive indices have been precisely measured with a 2WAJ Abbe refractometer at the wavelength of the VCSEL laser diode.

The phase signal, for each pixel i , recorded with mannitol can be expressed as:

$$\varphi_{1,i} = \frac{2\pi}{\lambda} (\bar{n}_{c,i} - n_m) h_i \quad (1)$$

and with Nycodenz as:

$$\varphi_{2,i} = \frac{2\pi}{\lambda} (\bar{n}_{c,i} - (n_m + \delta n)) h_i \quad (2)$$

where n_m and $n_m + \delta n$ are the refractive indices of the two different perfusion solutions, h_i the cell thickness and $\bar{n}_{c,i}$ is the integral refractive index defined as the mean value of the intracellular refractive index along the cell thickness h_i (Rappaz et al., 2005). By solving this equation system, the $\bar{n}_{c,i}$ and h_i values, for each pixel i , are obtained (Figure 2).

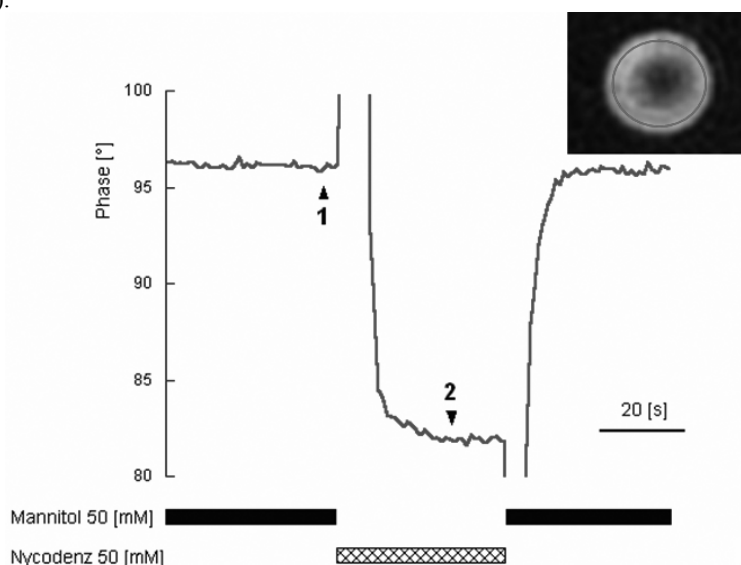


Figure 2: Principle of the decoupling procedure. Comparison of the phase signal recorded in (1) and (2) allow to obtain an independent measure of the refractive index and the thickness of the erythrocyte.

However, in order to minimize the effect of erythrocyte micromovements occurring over the 30 second solution exchange time, the h_i values has been calculated by using, as a first approximation, the mean cell integral refractive index $\bar{n}_c = \frac{1}{N_c} \sum_{i=0}^{N_c} n_{c,i}$ rather than $\bar{n}_{c,i}$ (Rappaz et al., 2005). As far as red blood cells are concerned, the mean refraction index measurements of different erythrocyte regions do not present statistically significant spatial variations. Such a spatially homogeneous intracellular refractive index is consistent with a homogeneous erythrocyte cytoplasm containing no organelle and strengthens the appropriateness of the \bar{n}_c approximation.

VOLUME MEASUREMENT

Figure 3 shows a topographic representation of a few erythrocytes after having performed the decoupling procedure. The classical biconcave shape can be observed. Table 1 presents the mean values of the refractive index and volume for a 13-erythrocyte sample.

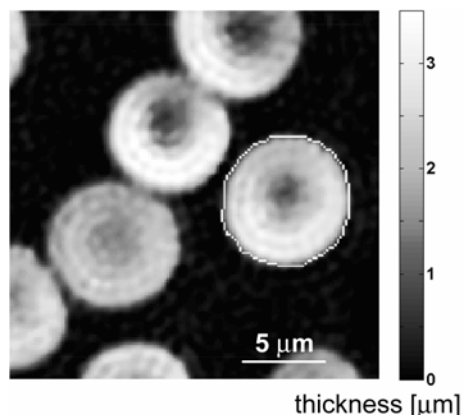


Figure 3: Topographic representation of erythrocytes. The mean refractive index and the measured volume of the cell are: $n = 1.401$ and $v = 109 \mu\text{m}^3$, respectively. The cell contour (white line) is determined by a classical gradient-based edge detection algorithm.

The mean refractive index value lies within the range of previously measured values of 1.37 to 1.42 by (Curl et al., 2005; Evans and Fung, 1972; Hammer et al., 1998; Mazon et al., 1997). On the other hand, despite the small erythrocyte sample size (n=13), the mean erythrocyte volume measured is in good agreement with the erythrocyte volume distribution obtained with a routine Coulter counter method (Bessman and Johnson, 1975) and quite close to the typical erythrocyte volume value given in textbooks ($92 \pm 9 \mu\text{m}^3$, (Lewis et al., 2001).

	Refractive Index	Volume [μm^3]
erythrocytes	1.394 ± 0.008	106 ± 15
neurons	1.380 ± 0.007	n.d.

Table 1: Measured refractive index of erythrocytes (n = 13) and neurons (Rappaz et al., 2005), expressed as mean \pm SD. n.d. not determined

We stress that this technique allows to measure the mean integral refractive index of living specimen with an excellent precision of 0.0003. The refractive index is a biophysical property of the cell related to the intracellular content, in particular to the intracellular proteins concentration which largely determines its value (Tycko et al., 1985). Specifically, as far as erythrocytes are concerned, the intracellular refractive index is mainly determined by the cell hemoglobin concentration, a parameter altered in various pathological states (Mohandas and Evans, 1994).

In Table 1, the erythrocyte refractive index is also compared with the refractive index of living neurons in culture measured with the same procedure (Rappaz et al., 2005). The comparatively large erythrocyte refractive index value results from the hemoglobin concentration.

CELL MEMBRANE FLUCTUATIONS

To assess the amplitude of membrane fluctuations, we have compared the temporal fluctuation of the phase signal of a region within the erythrocyte versus a region outside the erythrocyte, serving as a control signal. A control experiment with a confocal microscope showed that the lower membrane of the cell is attached to the glass coverslip and thus does not contribute to membrane fluctuations (data not shown).

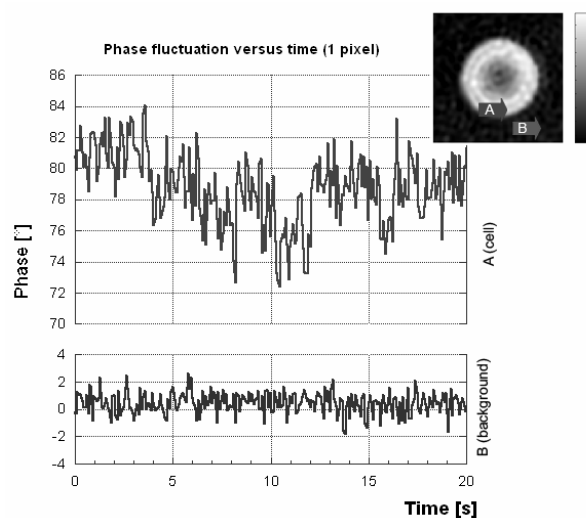


Figure 4 : Phase signals of two different regions (1 pixel region outside the cell (B, bottom) and within the cell (A, top)) recorded during at 13 Hz during a 10s period. The standard deviations of the signal are 0.44° and 1.37° , respectively.. Inset: phase image of the monitored erythrocyte with the corresponding regions indicated by color arrows.

Phase signals were recorded during 10s on two different regions of 4×4 pixels (to minimize artifact due to lateral micromovements of the cell), one outside the cell (arrow B, reference) and one in the central region of the cell (arrow A). Membrane fluctuation is measured in term of temporal phase variation. The standard deviations of those two temporal phase signals are 0.44° and 1.37° , respectively, indicating membrane fluctuation amplitude larger than the background noise level. This phase deviation fluctuations being measured for each pixel image, the temporal variation of any cell regions (cell rim, microdomains, etc.) can be simultaneously assessed. Using

this approach, we compared the temporal phase fluctuations of living erythrocyte versus fixed erythrocyte. For this experiment, cells have been monitored at ~ 13 Hz for 10s. Practically, on the images presented in Figure 5 each pixel corresponds to the temporal standard deviation of the phase signal over a 10s time period.

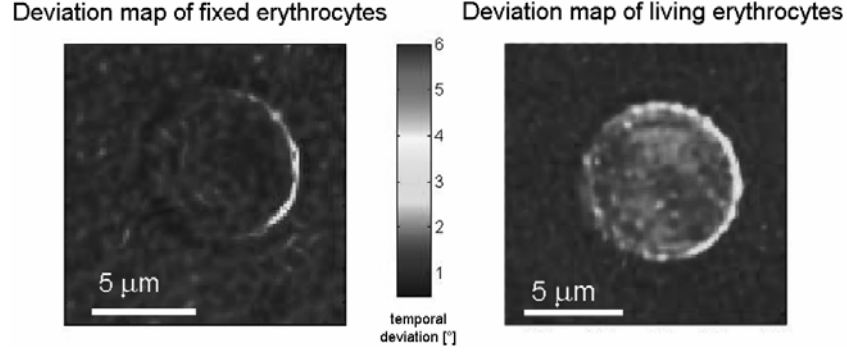


Figure 5 : Deviation map for fixed (left) and living (right) erythrocytes. The colorbar indicates the temporal standard deviation for every pixel of the phase image during the 10s recording period.

The left image shows the temporal standard deviation of the phase signal for fixed cell and the right images for living cells. In order compare the two conditions, we have defined two areas: the center of the cell defined as all the pixels lying within a $3\mu\text{m}$ diameter disk centered in the middle of the cell and the background corresponding to all the pixels outside the cells farther than $\sim 2\mu\text{m}$ from the cells edge. On the left image, fixed cell bodies, except edge areas, exhibit the same fluctuation amplitudes as the fluctuation amplitudes of areas outside the cells (temporal phase deviation = 0.95° and 0.97° , respectively, t-test: $p=0.68$, $n=4$) corresponding to the experimental phase stability. In contrast, the right images (living cells), show that the fluctuation amplitudes of the cell central regions are larger than those corresponding to areas outside the cells (temporal phase deviation = 1.8° and 1.1° , respectively, t-test: $p=0.0003$, $n=4$).

A rather constant phase temporal deviation is observed over the cell surface except for the cell border regions. The larger edge fluctuation amplitudes, also seen on fixed cells, corresponds to a small lateral displacement of the cell during the recording period and to the diffraction pattern of the cell rim (which can be also be observed in phase images, like in Figure 4).

The fluctuation phase signal recorded in the centre of the cell depends on both the parasitic phase fluctuations (associated to perfusion liquid movement or vibration, noise from the CCD camera, air turbulence, etc.), measured outside the cell areas, and on the actual membrane fluctuations. Consequently, the temporal variance of the phase signal recorded in the cell central regions, $Var(\varphi_{cell} + \varphi_{background})$, can be expressed by:

$$Var(\varphi_{cell} + \varphi_{background}) = Var(\varphi_{cell}) + Var(\varphi_{background}) + 2Cov(\varphi_{cell}, \varphi_{background}), \quad (3)$$

where, $Var(\varphi_{cell})$, $Var(\varphi_{background})$ are the temporal variance corresponding to the cell membrane fluctuations and to the parasitic phase fluctuation respectively, $Cov(\varphi_{cell}, \varphi_{background})$ is the covariance of the two variables.

Assuming that the two variables are independent, $Cov(\varphi_{cell}, \varphi_{background}) = 0$, which is a proper hypothesis as far as weakly diffracting object including living cells are considered. Thus, equation (3) can be simplified and the standard deviation of the cell membrane can be evaluated by:

$$std(\varphi_{cell}) = \sqrt{(std(\varphi_{cell} + \varphi_{background}))^2 - (std(\varphi_{background}))^2} \quad (4)$$

The resulting value is a temporal phase deviation of $1.42 \pm 0.18^\circ$ ($n = 4$ cells). Considering the measured mean refractive index of the erythrocytes in our experimental conditions (1.394), this phase deviation corresponds to a membrane fluctuation of 43.9 ± 5.4 nm (mean \pm STD). This value is in good agreement with previously measured values of 52.6 nm (Bitler et al., 1999), 46.8 nm (Popescu et al., 2006) and (Brochard and Lennon, 1975).

CONCLUSION

Digital holography microscopy (DHM) is a technique that allows to obtain, from a single recorded hologram, quantitative phase images of living cell dynamics with a nanometric axial accuracy. The quantitative phase images, containing information about both the cell morphometry and the integral refractive index, can be

unambiguously interpreted thanks to the decoupling procedure presented here. In addition, DHM, thanks to its subwavelength phase shift measurements, was found to yield an efficient tool to assess erythrocyte cell membrane fluctuations (ECMF). Typically, ECMF characterized by an amplitude within the range of 45 nm were observed.

The measures of the erythrocyte volume, refractive index and cell membrane fluctuations provide insight into the biophysical properties and physiological state of the red blood cells altered in different blood diseases.

This study was supported by the Swiss National Science Foundation (grant n° 205320-112195/1).

REFERENCES

- Barer, R. 1957. Refractometry and Interferometry of Living Cells. *Journal of the Optical Society of America* 47(6):545-556.
- Bessman, J.D., and R.K. Johnson. 1975. Erythrocyte Volume Distribution in Normal and Abnormal Subjects. *Blood* 46(3):369-379.
- Bitler, A., A. Barbul, and R. Korenstein. 1999. Detection of movement at the erythrocyte's edge by scanning phase contrast microscopy. *Journal of Microscopy-Oxford* 193:171-178.
- Brochard, F., and J.F. Lennon. 1975. Frequency Spectrum of Flicker Phenomenon in Erythrocytes. *Journal De Physique* 36(11):1035-1047.
- Colomb, T., E. CuChe, F. Charriere, J. Kuhn, N. Aspert, F. Montfort, P. Marquet, and C. Depeursinge. 2006. Automatic procedure for aberration compensation in digital holographic microscopy and applications to specimen shape compensation. *Applied Optics* 45(5):851-863.
- CuChe, E., P. Marquet, and C. Depeursinge. 1999. Simultaneous amplitude-contrast and quantitative phase-contrast microscopy by numerical reconstruction of Fresnel off-axis holograms. *Appl Opt* 38(34):6994-7001.
- Curl, C.L., C.J. Bellair, T. Harris, B.E. Allman, P.J. Harris, A.G. Stewart, A. Roberts, K.A. Nugent, and L.M. Delbridge. 2005. Refractive index measurement in viable cells using quantitative phase-amplitude microscopy and confocal microscopy. *Cytometry A* 65(1):88-92.
- Evans, E., and Y.C. Fung. 1972. Improved Measurements of Erythrocyte Geometry. *Microvascular Research* 4(4):335-&.
- Hammer, M., D. Schweitzer, B. Michel, E. Thamm, and A. Kolb. 1998. Single scattering by red blood cells. *Applied Optics* 37(31):7410-7418.
- Lewis, S.M., B.J. Bain, and I. Bates. 2001. Dacie and Lewis practical haematology, 9th ed. Churchill Livingstone.
- Marquet, P., B. Rappaz, P.J. Magistretti, E. CuChe, Y. Emery, T. Colomb, and C. Depeursinge. 2005. Digital holographic microscopy: a noninvasive contrast imaging technique allowing quantitative visualization of living cells with subwavelength axial accuracy. *Opt Lett* 30(5):468-470.
- Mazeron, P., S. Muller, and H. ElAzouzi. 1997. Deformation of erythrocytes under small-angle light scattering study. *Biorheology* 34(2):99-110.
- Mohandas, N., and E. Evans. 1994. Mechanical-Properties of the Red-Cell Membrane in Relation to Molecular-Structure and Genetic-Defects. *Annual Review of Biophysics and Biomolecular Structure* 23:787-818.
- Popescu, G., T. Ikeda, R.R. Dasari, and M.S. Feld. 2006. Diffraction phase microscopy for quantifying cell structure and dynamics. *Opt Lett* 31(6):775-777.
- Rappaz, B., P. Marquet, E. CuChe, Y. Emery, C. Depeursinge, and P.J. Magistretti. 2005. Measurement of the integral refractive index and dynamic cell morphometry of living cells with digital holographic microscopy. *Optics Express* 13(23):9361-9373.
- Tycko, D.H., M.H. Metz, E.A. Epstein, and A. Grinbaum. 1985. Flow-Cytometric Light-Scattering Measurement of Red Blood-Cell Volume and Hemoglobin Concentration. *Applied Optics* 24(9):1355-1365.